Chemistry of Metals and Alloys

Chem. Met. Alloys 12 (2019) 51-60
Ivan Franko National University of Lviv
www.chemetal-journal.org

Phase equilibria between the quaternary semiconductors $A^{I}_2B^{II}C^{IV}X_4$ (A^{I} – Cu; B^{II} – Zn, Cd; C^{IV} – Si, Ge, Sn, X – S, Se)

I.D. OLEKSEYUK[1], L.P. MARUSHKO[1], I.A. IVASHCHENKO[1]*, L.V. PISKACH[1], O.V. PARASYUK[1]

[1] *Department of Chemistry and Technology, Lesya Ukrainka Eastern European National University, Voli Ave. 13, 43025 Lutsk, Ukraine*
* *Corresponding author. E-mail: inna.ivashchenko05@gmail.com*

Received October 10, 2019; accepted December 18, 2019; available on-line April 1, 2020
https://doi.org/10.30970/cma12.0387

The interactions between quaternary compounds $A^{I}_2B^{II}C^{IV}X_4$ have been investigated. For the Cu_2CdGeS_4–Cu_2CdSnS_4 and $Cu_2ZnGeSe_4$–$Cu_2CdGeSe_4$ systems polythermal sections were constructed. In the zinc-containing systems, the extent of the solid solutions based on the end compounds were investigated. The largest solid solution width was observed along the Cu_2ZnGeS_4–Cu_2ZnSiS_4 section, where Cu_2ZnSiS_4 extends up to 50 mol.%.

Chalcogenides / Semiconductors / X-ray diffraction / Crystal structure

1. Introduction

Numerous reports on the crystal chemical and physical properties of quaternary chalcogenide semiconductors and their solid solutions have been published in recent years [1-9] to find materials with better electrical, optical, and magnetic properties than well-known binary or ternary compounds. Quaternary chalcogenides are also actively used to create more efficient solar cells. Using solid solutions based on them, it is possible to modify the physical properties of the materials in the desired direction [10-15]. But in such complex systems containing five elements, understanding the features of the crystal structure is especially important for a correct interpretation of the physical properties. In this article we report the results of an investigation of the solid solutions in the following systems: Cu_2CdGeS_4–Cu_2CdSnS_4, $Cu_2ZnGeSe_4$–$Cu_2CdGeSe_4$, Cu_2ZnGeS_4–Cu_2ZnSnS_4, Cu_2ZnGeS_4–Cu_2ZnSiS_4, Cu_2ZnSnS_4–Cu_2ZnSiS_4, and their selenide analogs $Cu_2ZnGeSe_4$–$Cu_2ZnSnSe_4$, $Cu_2ZnGeSe_4$–$Cu_2ZnSiSe_4$, Cu_2ZnSnS_4–$Cu_2ZnSiSe_4$. The listed sections were primarily studied to determine the boundaries of the solid solution ranges of the end compounds. The results of the study will allow us to evaluate the prospects of further, deeper studies, with a view to suggest practical applications in modern semiconductor industry.

2. Experimental

For every system, several alloys were synthesized from high-purity elements in evacuated quartz ampoules using the direct single-temperature method. The maximum synthesis temperature varied depending on the melting points of the end compounds. After the first stage of the synthesis, the alloys were ground into powder and pressed into tablets. The samples were annealed at 1070 K for 70 h, the procedure being repeated up to three times for some samples that were not single-phase. Then all the alloys were annealed at 670 K for 500 h followed by quenching into water at room temperature. The obtained samples were investigated by XRD (DRON 4-13 diffractometer, Cu$K\alpha$ radiation) and differential thermal analysis. The DTA curves were recorded using Pt/Pt-Rh thermocouples in a combination of a "Thermodent" regulated-heating furnace and a H307-1 *XY* recorder set. The speed of heating was 10 K/min. In a few cases recording was repeated with a speed of 3 or 7 K/min (after repeated anneal for 100 h at 670 K). As reference standard Al_2O_3 calcined at 1270 K for 10 h was selected. We used Cu, Ag, Ge, NaCl, Sb, Te, Cd, and Sn for calibration. All of the samples were investigated in quartz ampoules evacuated to 0.1 Pa.

3. Results and discussion

3.1. The Cu_2CdGeS_4–Cu_2CdSnS_4 section

The vertical section of the Cu_2CdGeS_4–Cu_2CdSnS_4 system was investigated by XRD and DTA (Fig. 1). The section liquidus is represented by the primary crystallization curves of the solid solutions ε (curve *ab*) and β (curve *bc*). The section crosses the plane of the invariant process of transition type L+β⇆δ+ε at 1187 K forming the horizontal line *de*. The regions of co-existence of the three phases L+β+ε (field 4) and L+β+δ (field 5) converge to this horizontal. Below, the region of the monovariant eutectic process L⇆δ+ε and the region of the monovariant peritectic process L+ε⇆γ converge to the segment *fg*. This horizontal belongs to the plane of the invariant process of transition type L+ε⇆γ+δ, which takes place at 1176 K. The segment *fg* coincides with the connecting line of this plane, therefore the alloys of this section are two-phase (γ+δ) below 1176 K.

At this temperature, the extent of the γ-solid solution is 11 mol.% Cu_2CdSnS_4, and that of the δ-solid solution is 16 mol.% Cu_2CdGeS_4. The solid solution range changes little with decreasing temperature, and reaches 9 mol.% for the γ-solid solutions and 14 mol.% for the δ-solid solutions at 670 K. The boundaries of the solid solutions at the annealing temperature were determined by plotting the change of the unit-cell parameters (Fig. 2).

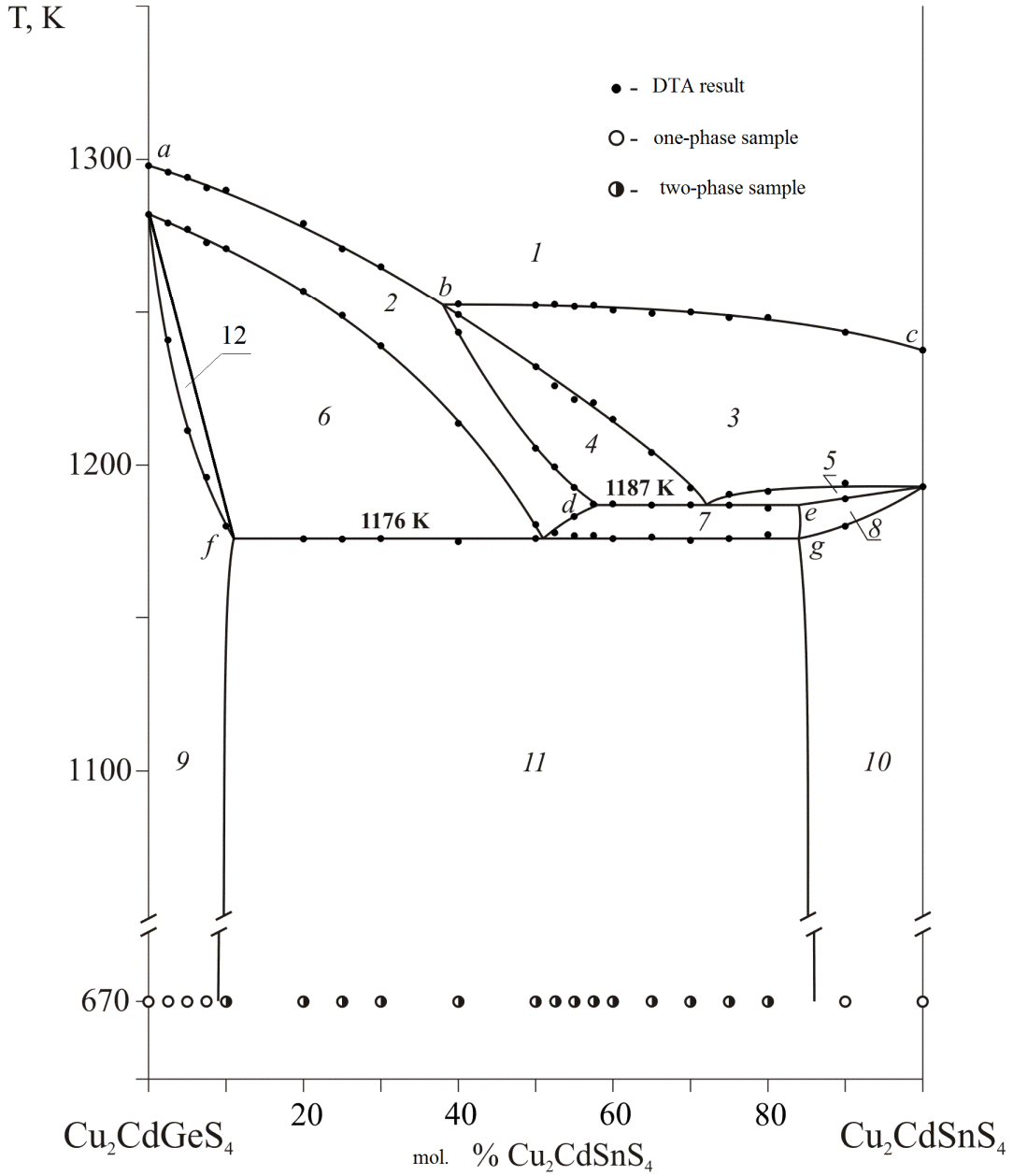

Fig. 1 Vertical section Cu_2CdGeS_4–Cu_2CdSnS_4: 1 – L; 2 – L+ε; 3 – L+β; 4 – L+β+ε; 5 – L+β+δ; 6 – L+γ+ε; 7 – L+δ+ε; 8 – L+δ; 9 – γ; 10 – δ; 11 – γ+δ; 12 – L+γ.

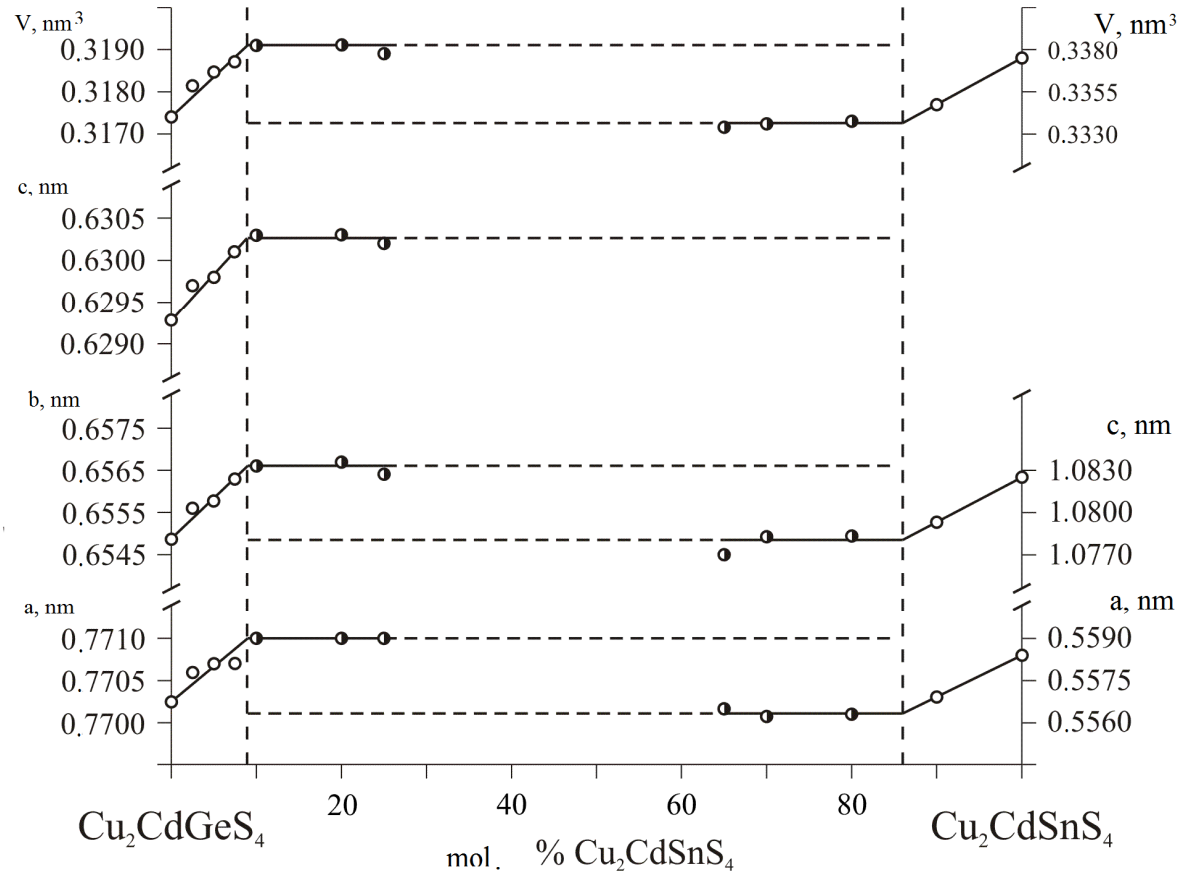

Fig. 2 Variation of the unit-cell parameters for the Cu_2CdGeS_4–Cu_2CdSnS_4 section.

3.2. The $Cu_2ZnGeSe_4$–$Cu_2CdGeSe_4$ section

The $Cu_2ZnGeSe_4$ compound, which forms in the Cu_2GeSe_3–ZnSe system, melts incongruently at 1163 K and has a polymorphous transition in the temperature range 1060–1077 K from a tetragonal low-temperature modification (LTM) to a high-temperature modification (HTM) with unknown crystal structure [16]. $Cu_2CdGeSe_4$ forms in the Cu_2GeSe_3–CdSe system *via* the peritectic reaction $L+Cu_2Cd_3GeSe_6 \leftrightarrows Cu_2CdGeSe_4$ at 1103 K. This compound has two polymorphous modifications, the orthorhombic HTM (space group $Pmn2_1$, a = 0.80968, b = 0.68929, c = 0.66264 nm) and the tetragonal LTM (space group I-42m, a = 0.57482, c = 1.10533 nm) [17]. According to the authors of [18], the polymorphous transition takes place at 878 K.

According to XRD data, $Cu_2ZnGeSe_4$ and $Cu_2CdGeSe_4$ form a continuous solid solution series with tetragonal structure at 720 K (Fig. 3). $Cu_2ZnGeSe_4$ crystallizes in I-42m with the unit-cell parameters a = 0.5607, c = 1.1042 nm, and LT-$Cu_2CdGeSe_4$ was indexed in the same space group with the unit-cell parameters a = 0.5749, c = 1.1055 nm, which are in good agreement with the literature data [16,17]. The unit-cell parameter a and the unit-cell volume vary fairly linearly with the Zn/Cd ratio in the $Cu_2Zn_{1-x}Cd_xGeSe_4$ solid solutions (Fig. 4), while the parameter c shows deviation from a straight line, with a maximum at x = 0.7. The variation of the unit-cell volume agrees well with the sizes of the cations involved in the substitution, Zn^{2+} (0.074 nm) and Cd^{2+} (0.092 nm). As the zinc content increases, the parameter of tetragonal distortion ($\Delta = 2 - c/a$) increases (Fig. 4), which is manifested in greater splitting of particular reflections in the diffraction patterns (Fig. 3). Results of the X-ray diffraction investigation of the solid solutions '$Cu_2Zn_{0.5}Cd_{0.5}GeSe_4$' and '$Cu_2Zn_{0.3}Cd_{0.7}GeSe_4$' are summarized in Tables 1 and 2.

The vertical section Cu_2CdGeS_4–Cu_2CdSnS_4 was built from DTA. The liquidus consists of the two curves of primary crystallization of the ε-solid solution range of ZnSe and the ζ-solid solutions of $Cu_2Cd_3GeSe_6$. The horizontal line at 1110 K belongs to the invariant peritectic process $L+\varepsilon \leftrightarrows \beta+\zeta$ that takes place in the Cu_2GeSe_3–ZnSe–CdSe system. There are two continuous solid solution series, the β-solid solutions of the HT modifications of the quaternary compounds, and the α-solid solutions of their LT modifications (Fig. 5).

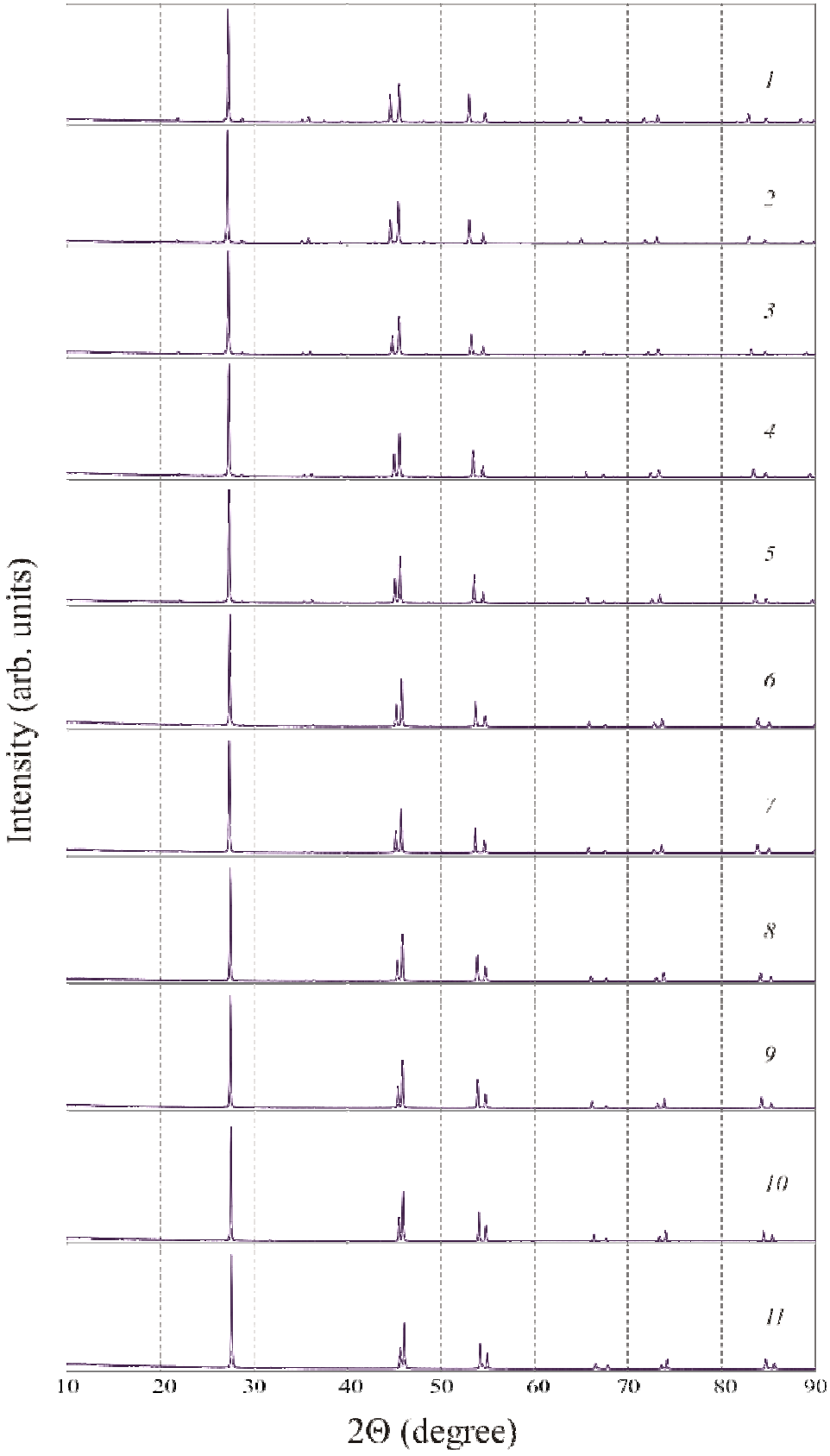

Fig. 3 Experimental diffraction patterns of the samples of the $Cu_2ZnGeSe_4$–$Cu_2CdGeSe_4$ section.

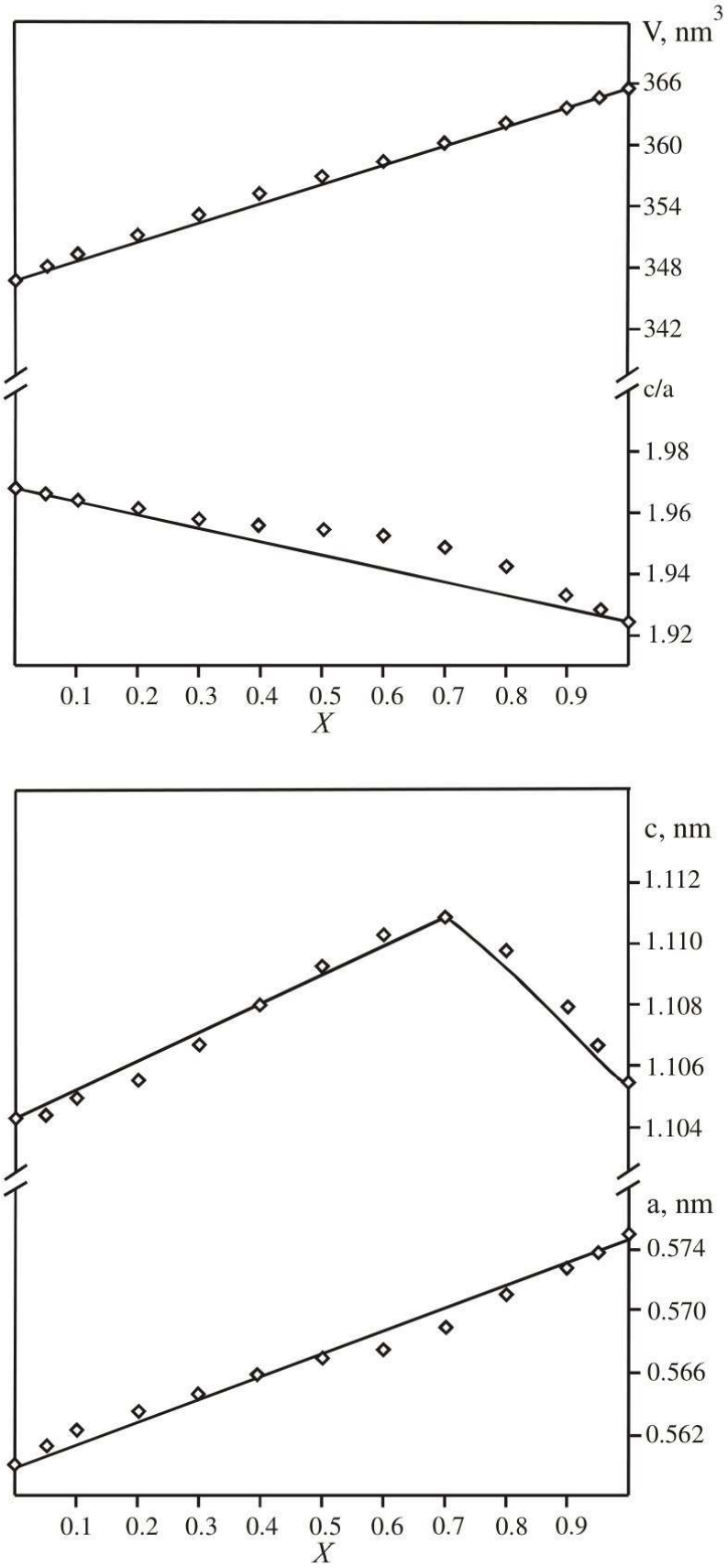

Fig. 4 Unit-cell parameters in the system $Cu_2Zn_{1-x}Cd_xGeSe_4$ (tetragonal crystal structure, space group *I*-42*m*).

Table 1 Results of the refinement of the crystal structure of the solid solutions '$Cu_2Zn_{0.5}Cd_{0.5}GeSe_4$' and '$Cu_2Zn_{0.3}Cd_{0.7}GeSe_4$'.

Formula	'$Cu_2Zn_{0.5}Cd_{0.5}GeSe_4$'	'$Cu_2Zn_{0.3}Cd_{0.7}GeSe_4$'
Formula units per unit cell	2	2
Space group	*I*-42*m*	*I*-42*m*
a (nm)	0.56831(3)	0.56940(1)
c (nm)	1.10904(6)	1.11248(3)
Unit-cell volume (nm^3)	0.35820(5)	0.36068(3)
Number of atoms in the cell	16	16
Calculated density (g/cm^3)	5.6033(8)	5.6513(4)
Absorption coefficient (1/cm)	519.46	556.43
Radiation, wavelength	Cu*K*α, 0.154185 nm	
Diffractometer	Powder DRON 4-13	
Mode of refinement	Full profile	Full profile
Number of atom sites	4	4
Number of free parameters	9	9
$2\theta_{max}$ (°); $\sin\theta / \lambda_{max}$ (1/nm)	100.02; 4.97	100.02; 4.97
R_I; R_p	0.0683; 0.1426	0.0782; 0.1092
Texture axis and parameter	[011] and 2.49(9)	[110] and 1.31(4)

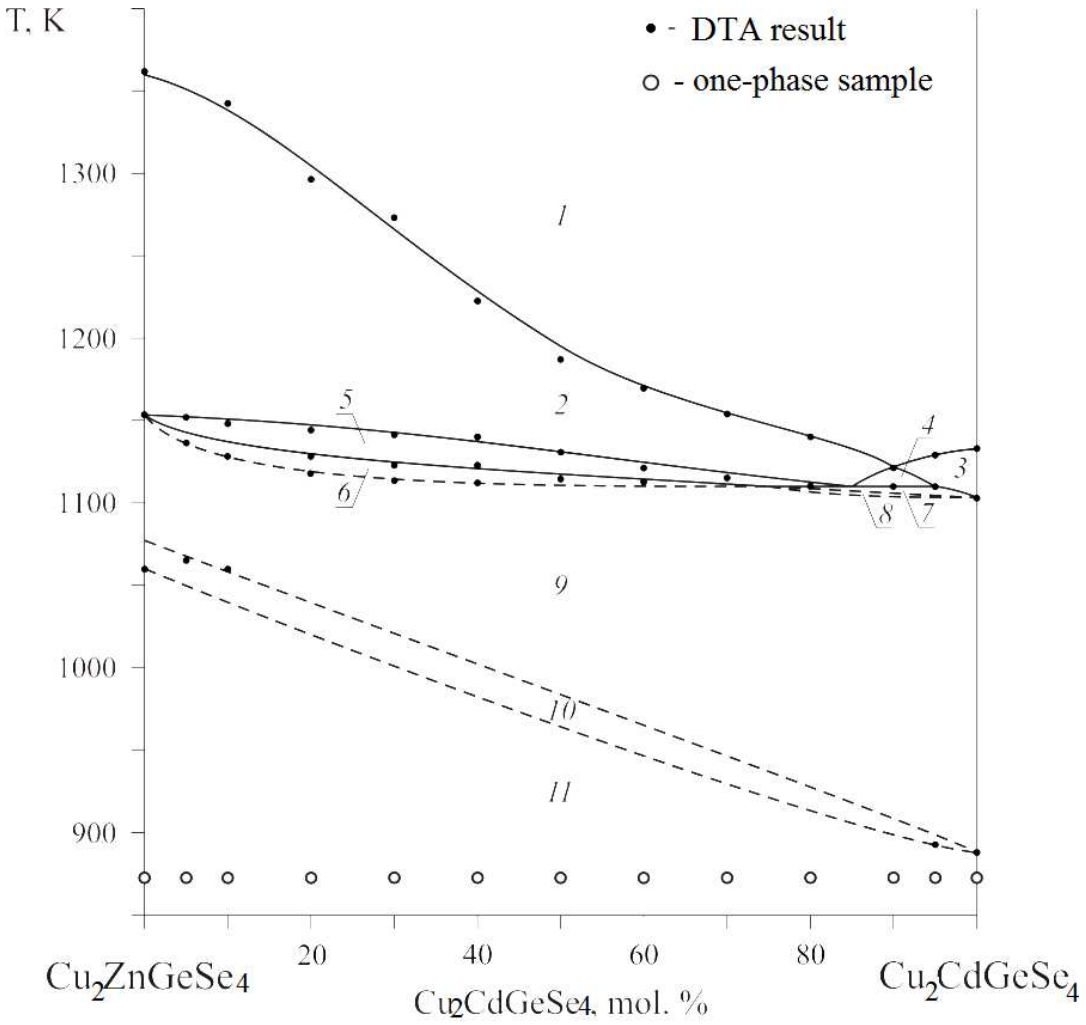

Fig. 5 Vertical section $Cu_2ZnGeSe_4$–$Cu_2CdGeSe_4$: 1 – L; 2 – L+ε; 3 – L+β; 4 – L+β+ε; 5 – L+β+δ; 6 – L+γ+ε; 7 – L+δ+ε; 8 – L+δ; 9 – γ; 10 – γ+δ; 11 – δ.

Table 2 Atom coordinates and isotropic displacement parameters in the structures of the solid solutions '$Cu_2Zn_{0.5}Cd_{0.5}GeSe_4$' and '$Cu_2Zn_{0.3}Cd_{0.7}GeSe_4$' (space group *I*-42*m*).

Atom	Wyckoff site	*x*	*y*	*z*	Occupation	$B_{iso}\times10^2$ nm^2
'$Cu_2Zn_{0.5}Cd_{0.5}GeSe_4$'						
Cu	4*d*	½	0	¼	1	0.69(13)
M	2*a*	0	0	0	0.5 Zn+0.5 Cd	1.1(2)
Ge	2*b*	0	0	½	1	0.35(15)
Se	8*i*	0.2672(2)	0.2672(2)	0.1279(2)	1	1.21(11)
'$Cu_2Zn_{0.3}Cd_{0.7}GeSe_4$'						
Cu	4*d*	½	0	¼	1	1.16(5)
M	2*a*	0	0	0	0.3 Zn+0.7 Cd	1.89(6)
Ge	2*b*	0	0	½	1	1.70(8)
Se	8*i*	0.2649(1)	0.2649(1)	0.1313(1)	1	1.62(3)

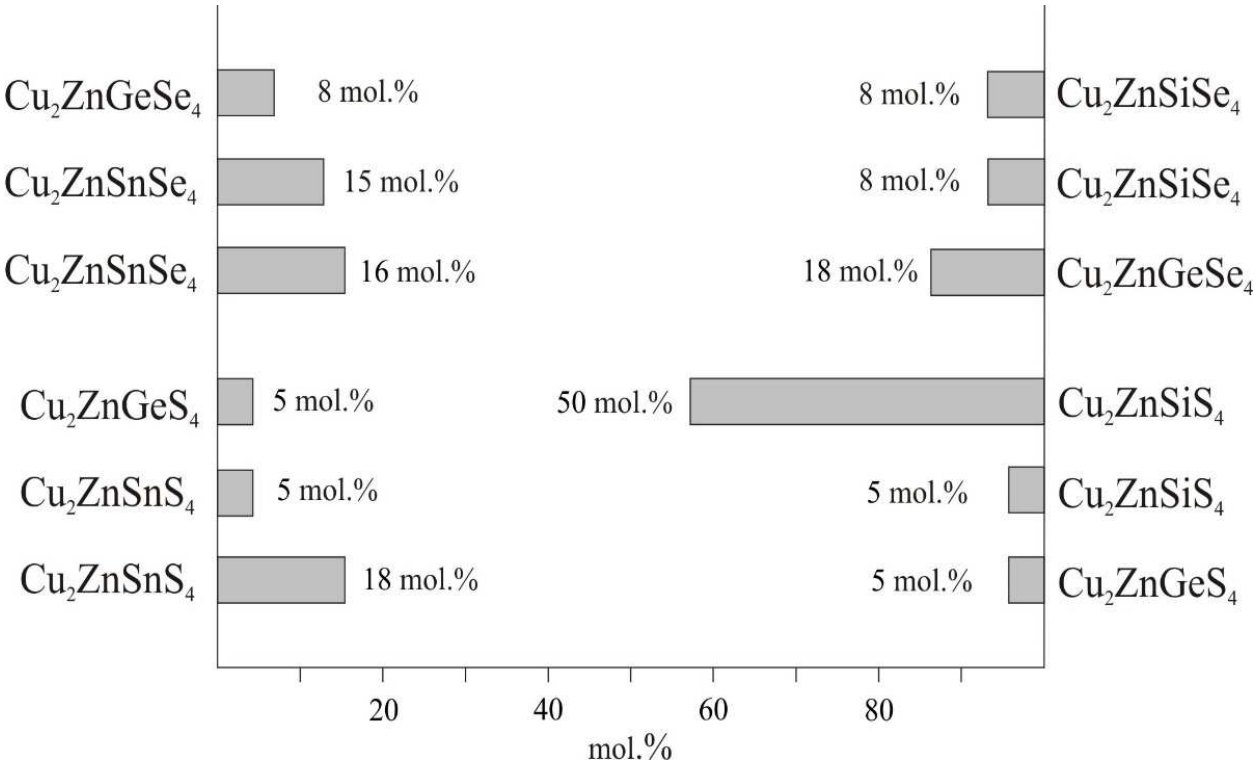

Fig. 6 Graphical representation of the extent of the solid solutions of the quaternary end compounds in the $Cu_2ZnC_1^{IV}X_4$–$Cu_2ZnC_2^{IV}X_4$ sections.

3.3. The Cu_2ZnGeS_4–Cu_2ZnSiS_4 and other $Cu_2ZnC_1^{IV}X_4$–$Cu_2ZnC_2^{IV}X_4$ sections (C_1, C_2 = Si, Ge, Sn, X = S, Se)

Despite the incongruent type of formation of the end compounds, the studied sections are quasi-binary in the solid state. They exhibit small solid-state solubility based on the quaternary compounds. The boundaries of these solid solutions were determined by plotting the variation of the unit-cell parameters (Figs. 6,7). In most cases, the extent was 5-15 mol.%. The mechanism of formation of solid solutions is the substitution of Si, Ge, Sn on their crystallographic site. No other redistribution of atoms was observed in the crystal structure.

A system of particular interest is the Cu_2ZnGeS_4–Cu_2ZnSiS_4 section, where the solubility based on Cu_2ZnSiS_4 reaches up to 50 mol.% Cu_2ZnGeS_4 (Fig. 7). For the '$Cu_2ZnSi_{0.5}Ge_{0.5}S_4$' composition (Fig. 8) the mechanism of formation of solid solutions in this system was studied. It is the substitution of germanium atoms for silicon on the crystallographic site 2*a* (Tables 3,4). The variation of the unit-cell parameters within this solid solution is linear, increasing to a = 0.7479, b = 0.6446, c = 0.6168 nm (Fig. 7).

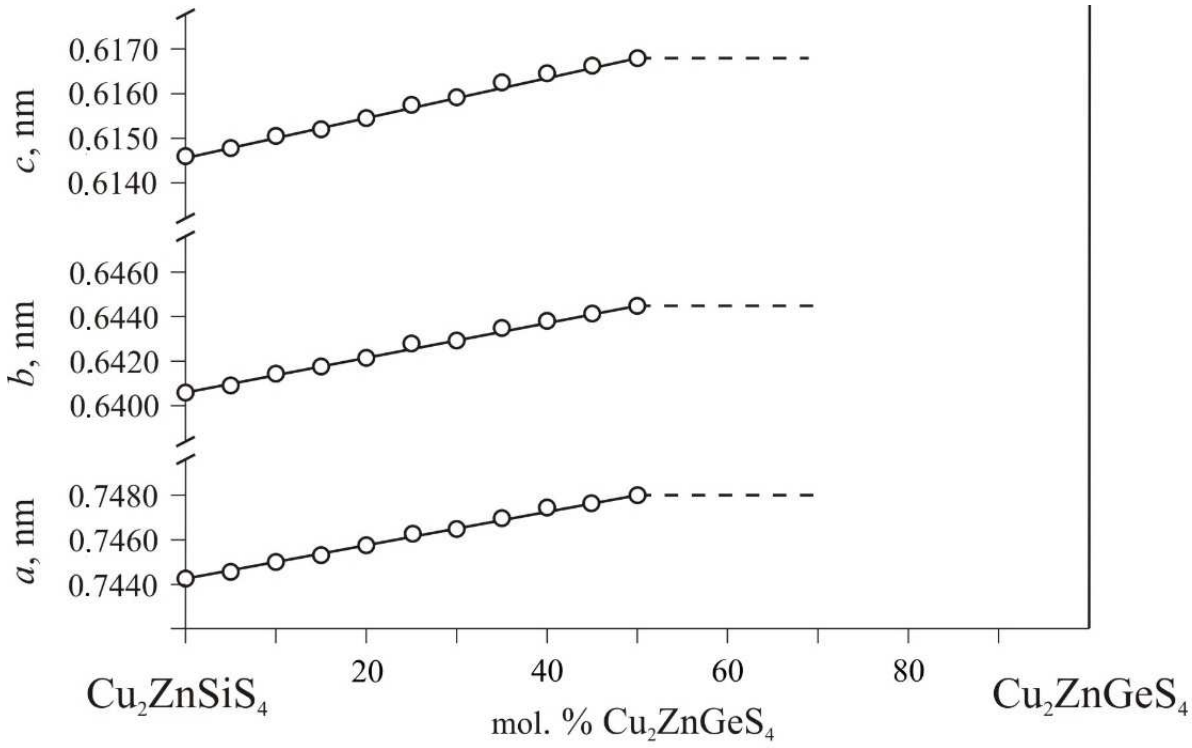

Fig. 7 Variation of the unit-cell parameters of the solid solutions of Cu_2ZnSiS_4 along the Cu_2ZnGeS_4–Cu_2ZnSiS_4 section.

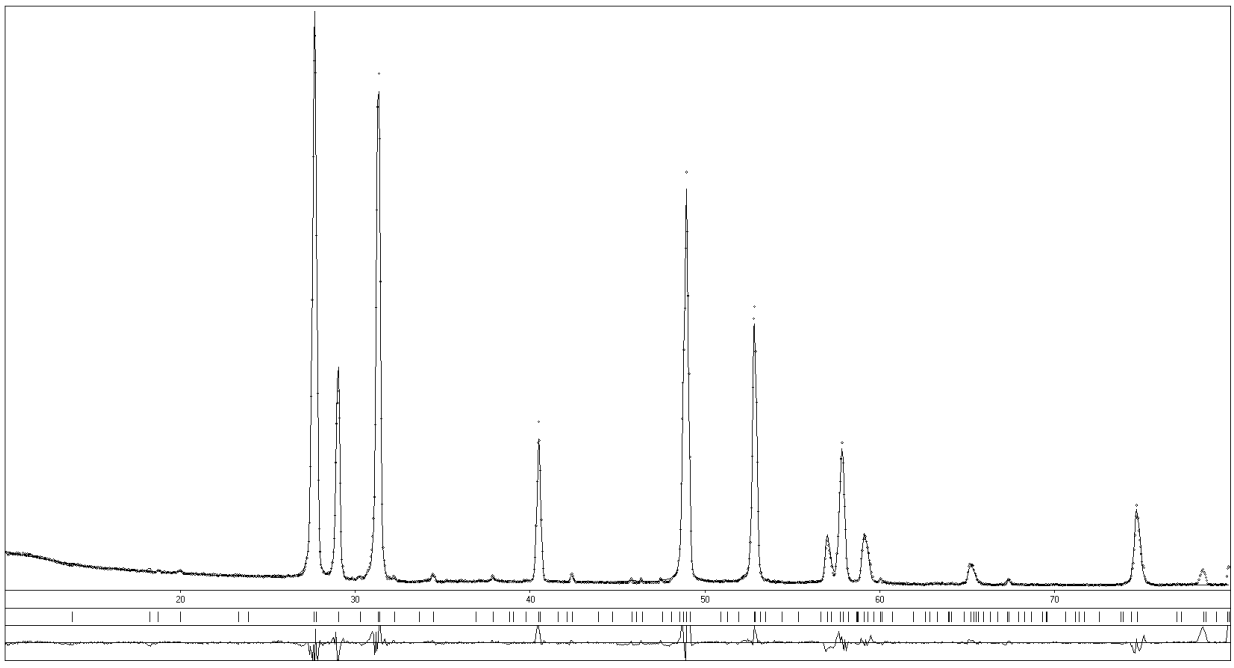

Fig. 8 Experimental and calculated diffraction patterns of the solid solution '$Cu_2ZnSi_{0.5}Ge_{0.5}S_4$' and their difference.

Table 3 Results of the structural refinement of the solid solution '$Cu_2ZnSi_{0.5}Ge_{0.5}S_4$' at the Cu_2ZnGeS_4-Cu_2ZnSiS_4 section.

Space group	$Pmn2_1$
a (nm)	0.74787(5)
b (nm)	0.64457(4)
c (nm)	0.61685(3)
Unit-cell volume (nm^3)	0.29735(5)
F(000) (electrons)	350
Number of atoms in the cell	16.0
Calculated density (g/cm^3)	4.1436(7)
Absorption coefficient (1/cm)	286.85
Radiation, wavelength	Cu*K*α, 0.154185 nm
Diffractometer	Powder
Mode of refinement	Full profile
Number of atom sites	6
Number of free parameters	22
$2\theta_{max}$ (°); $\sin\theta/\lambda_{max}$ (1/nm)	99.52; 4.95
R_I; R_p	0.0550; 0.0990
Texture axis and parameter	[330] and 0.268(8)

Table 4 Atom coordinates and isotropic displacement parameters in the structure of the solid solution '$Cu_2ZnSi_{0.5}Ge_{0.5}S_4$'.

Atom	Wyckoff site	*x*	*y*	*z*	Occupation	$B_{iso}\times10^2$ nm^2
Cu1	4*d*	0.2533(5)	0.1662(10)	0.118(11)	1	1.01(3)
Zn1	2*a*	0	0.3373(12)	0.609(11)	1	1.19(3)
M	2*b*	0	0.6720(14)	0.106(11)	0.5 Si + 0.5 Ge	0.84(3)
S1	8*i*	0	0.314(2)	0.240(11)	1	1.11(3)
S2	8*i*	0	0.675(2)	0.783(11)	1	1.08(3)
S3	8*i*	0.2482(10)	0.1733(14)	0.259(11)	1	1.16(3)

References

[1] E. Moreno, M. Quintero, M. Morocoima, E. Quintero, P. Grima, R. Tovar, P. Bocaranda, G.E. Delgado, J.E. Contreras, A.E. Mora, J.M. Briceño, R. Avila Godoy, J.L. Fernandez, J.A. Henao, M.A. Macías, *J. Alloys Compd*. 468 (2009) 212-218.

[2] S. Schorr, H.-J. Hoebler, M. Tovar, *Eur. J. Mineral*. 19 (2007) 65-73.

[3] P. Bonazzi, L. Bindi, G.P. Bernardini, S. Menchetti, *Can. Mineral.* 41 (2003) 639-647.

[4] G.P. Bernardini, D. Borrini, A. Caneschi, F. Di Benedetto, D. Gatteschi, S. Ristori, M. Romanelli, *Phys. Chem. Miner*. 27 (2000) 453-461.

[5] E. Quintero, R. Tovar, M. Quintero, G.E. Delgado, M. Morocoima, D. Caldera, J. Ruiz, A.E. Mora, M. Briceño, J.L. Fernandez, *J. Alloys Compd*. 432 (2007) 142-148.

[6] D. Galdera, M. Quintero, M. Morocoima, E. Quintero, P. Grima, N. Marchan, E. Moreno, P. Bocaranda, G.E. Delgado, A.E. Mora, J.M. Briceño, J.L. Fernandez, *J. Alloys Compd*. 457 (2008) 221-224.

[7] E. Quintero, R. Tovar, M. Quintero, M. Morocoima, J. Ruiz, G. Delgado, J.M. Broto, H. Rakoto, *Physica B* 320 (2002) 384-387.

[8] L. Marushko, L.V. Piskach, O.V. Parasyuk, I.A. Ivashchenko, I.D. Olekseyuk, *J. Alloys Compd*. 484 (2009) 147-153.

[9] I.D. Olekseyuk, O.A. Husak, L.D. Gulay, O.V. Parasyuk, *J. Alloys Compd*. 367 (2004) 25-35.

[10] G.Ye. Davydyuk, I.D. Olekseyuk, O.V. Parasyuk, S.V. Voronyuk, O.A. Dzham, V.I. Pekhnyo, *Ukr. Fiz. Zh.* 51 (2006) 380-385.

[11] I.D. Olekseyuk, O.V. Parasyuk, O.M. Yurchenko, V.Z. Pankevych, V.I. Zaremba, R. Valiente, Y.E. Romanyuk, *J. Cryst. Growth* 279 (2005) 140-145.

[12] G.Ye. Davydyuk, O.V. Parasyuk, Ya.E. Romanyuk, S.A. Semenyuk, V.I. Zaremba, L.V. Piskach, J.J. Koziol, V.O. Halka, *J. Alloys Compd*. 339 (2002) 40-45.

[13] O.V. Parasyuk, Y.E. Romanyuk, I.D. Olekseyuk, *J. Cryst. Growth* 275 (2005) 159-162.
[14] E. Quintero, M. Quintero, E. Moreno, M. Morocoima, P. Grima, P. Bocaranda, J.A. Henao, J. Pinilla, *J. Alloys Compd*. 471 (2009) 16-20.
[15] M. Altosaar, J. Raudoja, K. Timmo, M. Danilson, M. Grossberg, J. Krustok, E. Mellikov, *Phys. Status Solidi A* 205 (2008) 167-170.
[16] E. Parthé, K. Yvon, R.H. Deitch, *Acta Crystallogr., Sect. B* 25 (1969) 1164.
[17] O.V. Parasyuk, L.D. Gulay, Ya.E. Romanyuk, L.V. Piskach, *J. Alloys Compd*. 329 (2001) 202-207.
[18] L.V. Piskach, O.V. Parasyuk, Ya.E. Romanyuk, *J. Alloys Compd*. 299 (2000) 227-231.